Journal of Energy Storage 72 (2023) 108200

Contents lists available at ScienceDirect

Journal of Energy Storage

journal homepage: www.elsevier.com/locate/est

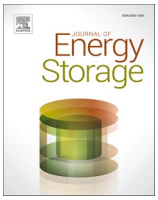

Research Papers

Towards more realistic Li-ion battery safety tests based on Li-plating as internal cell error

Ronald Gordon, Anna Smith *

Karlsruhe Institute of Technology (KIT), Institute for Applied Materials (IAM), Hermann-von-Helmholtz-Platz 1, D-76344 Eggenstein-Leopoldshafen, Germany

ARTICLE INFO

Keywords:
Li-ion battery
Battery safety
Li-plating
Realistic testing
Risk assessment

ABSTRACT

Herein the development of a novel test procedure for lithium ion cells to trigger cell internal defects under more realistic conditions (ambient temperature/voltage) than procedures that are currently used as triggers for propagation tests (e.g. nail penetration, massive heating/overcharge) is reported. Therefore, lithium plating, a common phenomenon of aging but also appearance of misbalanced/inhomogeneous cell construction, occurring within graphite-based lithium-ion battery cells, was chosen to be induced systematically and reproducibly by electrochemical cycling within different lithium-ion cell chemistries as well as pouch cell types (commercial and self-made). Using plating as a trigger method on different kind of test cells, showed that the behavior of cells differed, such that it is possible to classify the cells into categories based on the outcome of the test (e.g., swelling, venting, thermal runaway). Interestingly, not the lithium plating and dendrite growth through the separator itself but its consequences, such as degradation reactions with increase in inner resistance caused safety critical behavior of the cells. The test procedure can be applied on an electrically connected cell within a battery system and therefore has great potential to be used alternatively as a trigger method for the propagation test.

1. Introduction

Lithium-ion batteries (LIB) have been widely used as power supply in many applications, ranging from portable electronic devices over stationary short- and mid-term grid storage to electric vehicles, being the technology of choice to replace current fossil-fuel-based transportation technologies due to their high energy and power density [1–4]. In recent years, several advances regarding specific energy and power, cell lifetime and recyclability, reduced costs as well as environmental impact highlight the successful development of LIB, promoting its widespread commercialization. However, safety performance is still under scrutiny, diminishing LIB popularity under end-users and reasserting the necessity for battery regulation [5–11].

LIBs are expected to perform in a broad range of operating conditions, but when subjected to conditions outside their predefined window, they may fail through a variety of safety issues such as continuous gas and heat generation, eventually leading to cell rupture and ignition of combustible materials [12–15]. LIB safety is defined fundamentally by the fabrication process of the individual cells, as well as by the entire battery design and its reliability of components. Current, voltage and temperature are typically monitored at cell level by the battery management systems (BMS), which guarantee safe operation within the application window. BMS can immediately stop cell operation, if parameters outside this window are detected, i.e., overcharge/overdischarge, undercooling and overheating. Moreover, hard-case cells commonly have active safety features such as current interrupting devices (CID) and positive temperature coefficient (PTC) receptors, preventing the cell from elevated current, pressure or temperature [15]. Additionally, cooling concepts and mechanical shielding (housing) improve safety at battery level, resulting in an overall protected system, viz., electrically, mechanically and thermally. Nevertheless, internal cell errors, which may arise during proper cell operation usually cannot be detected in time and hence cannot be avoided by the aforementioned cell safety features.

Cell internal faults may originate from poor cell design and production issues including low electrode and separator quality, impurities or poor anode to cathode capacity balancing, stacking errors and, in general, inhomogeneities. Further, cells are bound to degrade during normal operation due to aging mechanisms such as decomposition of cell components, contact loss, particle break-up or formation of elemental Li due to solid-state diffusion limitations on the anode side, known as Li-plating [16–26]. Such cell faults may result in safety issues

* Corresponding author.
E-mail address: anna.smith@kit.edu (A. Smith).

https://doi.org/10.1016/j.est.2023.108200
Received 15 January 2023; Received in revised form 13 June 2023; Accepted 26 June 2023

including internal short-circuits, generally inducing a strong local heat generation, leading to possible gas formation, venting and potentially a self-accelerating exothermic reaction described as a thermal runaway (TR). Detection of these unpredictable safety risks during cell end-of-line tests or incoming goods inspections as well as prevention during proper cell operation is highly challenging, if not impossible. Despite internal errors being limited to cell level, their outcome can spread to neighboring cells (propagation), causing catastrophic failure at battery level [14,27–31]. Therefore, the impact of an internal cell fault is evaluated in testing standards by either introducing a trigger for an internal short-circuit, e.g., deliberate introduction of a nickel particle within the cell (IEC 62133-2:2017+AMD1:2021 CSV and IEC 62619:2022), which will perforate the separator upon application of external pressure, or manipulation of a small area of the separator by substitution with wax [32] that can easily melt under low heating conditions, both leading to an internal short circuit. However, such cell manipulation is rather difficult to implement during the fabrication process of a possibly fully automated production line and definitely challenging to implement after fabrication. Further, manipulated cells render mayor safety risks during transportation to a testing facility. Alternatively, the current choice for passing a safety test is to conduct a propagation test [10,11,33–40]. Thus, depending on the standard, during these procedures a cell within a battery module should be brought to the critical state of TR using specified or freely selectable methods including external heating, overcharging, nail or laser-beam penetration, a combination of these, or even further unspecified methods. Based on the standard, the exact procedure is usually selected by the battery testing facility. After initiation of the TR of one cell within a battery system the propagation is monitored. Depending on the field of battery application passing of the test is considered successful if certain criteria are met, e.g., according to DIN EN 62619 (VDE 0510-39:2017-11) no flames are allowed outside of the battery housing nor damage of the housing occurred for stationary application.

The ambiguous specifications and, particularly, the compulsory forced generation of TR as target even for relatively safe cells, render several disadvantages with respect to reproducibility, reliability, development and test costs, in addition to resulting test competitiveness. The methods used to trigger a TR in a single cell are virtually unrealistic as overcharge or overheating can be prevented by a properly functioning BMS and nails puncturing the cell describes a rather far-fetched scenario. High quality cells are generally less prone to errors and escalation thereof, forcing the testing facility to maltreat cells aggressively and thus unrealistically in order to trigger a TR, often with an introduction of massive external energy into the cell system. Accordingly, safer cells tend to be disadvantaged since they will take up more energy during abuse than low quality cells. Thus, battery modules build from more robust cells have to be over-dimensioned as they have to withstand larger amounts of energy release. Some higher quality cells in fact might not undergo a TR in the event of internal cell faults, even in a heavily aged state. Corresponding modules should be safeguarded against abuse that will not occur in practice in order to survive a TR induced under absurd conditions to meet the standards, unjustifiably increasing development costs. Currently, neither the test specifications in available standards for triggering TR, nor the possible implementation options in terms of accuracy, repeatability and meaningfulness are comparable. Certainly, more realistic test procedures to initiate cell internal errors and to evaluate their actual consequences at module level still need to be developed.

Li-plating represents a common internal cell fault, which may lead to safety-critical cell behavior. It is formed when the anode potential drops below 0 V vs. Li/Li^+ as an excessive number of Li-ions arrive at the anode surface, being unable to intercalate into the active material (mainly graphite) or diffuse inside the anode microstructure fast enough, resulting in a saturation of elemental Li on the anode surface [41–46]. Despite some of the plated Li being reused in the following cycle as it strips during the discharge step, the rest either reacts with the electrolyte or loses electrical contact, becoming “dead” Li, which translates to elevated internal cell resistance and capacity fade through loss of Li inventory [21,42,47–49]. In addition, large accumulations of Li can lead to Li dendrites. It has been reported that Li dendrite growth can result in a short-circuit as these metallic microstructures penetrate the separator and reach the cathode, potentially resulting in catastrophic cell failure [10,48–51]. Numerous research activities have dealt with the detection and characterization of Li-plating to better understand degradation pathways [50,52,53–68]. This detection techniques can be classified as local or global, direct or indirect, qualitative or quantitative, and *operando* vs. *in*/ex-situ. Even though these various techniques offer distinct advantages and allow for further knowledge aiming to better design LIB, their shortcomings including low precision, high complexity, poor practical implementation and steep cost limit their use under a technically relevant operational environment. Accordingly, Li-plating remains an unpredictable and potentially critical risk for cell safety.

This work presents the development of two test procedures based on the deliberate generation of Li-plating as realistic internal cell error. The reliability and reproducibility with respect to inducing Li-plating as trigger mechanism to safety-critical cell behavior is systematically evaluated and validated using different Li-ion cell chemistries (LFP: $LiFePO_4$, LCO: $LiCoO_2$, NMC: $LiNiCoMnO_2$, NCA: $LiNiCoAlO_2$) cathode active material vs. graphite-type anode material) and different pouch cell types, including self-made and commercial, that are based on liquid electrolyte. Considering the findings of both procedures, which follow a slight overcharge approach in either a controlled voltage or charge amount window, we propose a final, fine-tuned test procedure aimed to intensify its impact on the actual consequences to such a cell internal error. However, cells are not forced to undergo a TR, contrary to conventional propagation tests, even though particular cells are more prone to this outcome. Despite all studied cells exhibiting a similar characteristic response regarding cell parameters including cell potential and temperature, our results show that not Li-plating itself, but moreover its consequences (e.g., increase in inner resistance) lead to distinctive safety-critical cell behavior such as swelling, venting and even TR, allowing for risk assessment and cell categorization relating cell design/quality to test outcome. Accordingly, the developed test procedure offers not only new insights into the effect of Li-plating as internal cell error on cell safety performance, but also novel advances towards the implementation of more realistic test methods, which can be easily applied for cell and module testing and are effortlessly practicable in testing laboratories.

2. Experimental

2.1. Cell assembly of self-fabricated pouch cells and commercial cell specifications

Li-ion cells including different chemistries and formats were subjected to the test developed in this work. Cells in pouch format were built on the semi-automatic in-house production line of the KIT Battery Technology Center. Therefore, commercially available electrodes and separators based on different chemistries and composition were used to assemble the cells, respectively. Cathodes comprising $LiNi_{0.33}Mn_{0.33}Co_{0.33}O_2$ (NMC111, areal capacity of ~1.85 mAh/cm^2) as well as $LiNi_{0.6}Mn_{0.2}Co_{0.2}O_2$ (NMC622, areal capacity of 3.0 mAh/cm^2) as active material were employed. State of the art graphite-borne anodes with different capacities were matched with the corresponding cathode materials, so that 15–20 % overbalancing was achieved. For the separator, either trilayered PP/PE/PP or ceramic double-coated PET separators were used. A conventional EC:DMC 1:1 with 1 M $LiPF_6$ including 3 % VC as an additive was employed as the electrolyte. Single-layered lab-scale cells with a nominal capacity of 44 mAh (NMC111 based) as well as application-oriented multi-layered pouch cells with 10 Ah (NMC111 based) and 12 Ah (NMC622 based) were assembled and tested.

Moreover, commercially available state of the art cells with different

capacities were also subjected to the test: pouch-cells including an NMC-blend or NMC as cathode active material with a nominal capacity of 25 Ah or 50 Ah, respectively, were used. A cylindrical cell 18,650 based on NCA as active material with a nominal capacity of 3 Ah was employed for the investigation as well. Additionally, two hobby scene consumer pouch-cells comprising LFP or LCO as active material with nominal capacities of 3 Ah or 5 Ah, respectively, were used. A tabular summary of all investigated cells is provided in table S1 in the supporting information.

2.2. Testing equipment

Lab-scale cells were tested using a BioLogic VMP3 potentiostat, whereas self-assembled as well as commercial and consumer cells with higher nominal capacities were tested employing a BaSyTec MRS Battery Test System 6 V/300 A.

Cells with nominal capacities in the Ah-region render a higher risk in case of a safety-critical events. Hence, a sealed aluminum testing box was specially designed to carry out the measurements under safe conditions. The testing box was equipped with a check-valve connected to a high-performance toxic gas filter system for LIBs. A temperature-controlled stainless-steel plate connected to a cryostat was employed for temperature regulation inside the box. In addition, temperature sensors and thermal (IR) imaging cameras were equipped to register the temperature development on the surface of the cell. Depending on cell format, 2–4 thermal sensors were evenly attached to the surface of investigated cells, covering as much surface as possible. Accordingly, not only safety but also recording of critical parameters during the test can be guaranteed.

2.3. Test procedure for triggering Li-plating within cells

All cells were cycled at 3C constant current for 100 cycles. Directly after the last 3C-charge pulse, a 60-minute open-circuit-voltage (OCV) phase was applied in order to record the voltage relaxation of the cells over time and, ideally, to obtain initial indications of Li-plating in the course of the voltage drop, i.e., to be able to measure this as well. This set of 100 cycles followed by an OCV-phase was repeated 10 times for an equivalent total of 1000 cycles. For each test procedure, cells were cycled within a specific range of cell parameters, causing slight overcharge but incomplete discharge for sake of time:

- Voltage-controlled procedure: cycling between 3.6 V and 4.5 V

Cells were cycled within 3.6 and 4.5 V irrespective of the charge amount being charged or discharged at each cycle during the voltage-controlled procedure.

- State of charge (SOC)-controlled procedure: cycling between 70 % and 130 %

A specific charge amount was forced into and out of the cell independently of the cell-voltage using an Ah-counter during the SOC-controlled method. Initially, the amount of charge (Ah) supplied/extracted during a full charge/discharge step was recorded by the potentiostat via Ah-counter, defining the charge amount during the discharge step as cell capacity in the full SOC-range. Specific SOC values were set based on the initially determined capacity using an Ah-counter, i.e. amount of charge during charge/discharge.

- Definition of final version of most promising test procedure

After evaluation of the results obtained for both procedures, the most promising one regarding generation of safety-critical cell behavior was selected. Further, measurement parameters and test conditions were varied to fine-tune the test procedure and intensify its effect on the cell response, facilitating the classification of cells with different quality. The corresponding findings were used to define the final version of the most promising test procedure. This investigation will be discussed in the next section. The ultimate parameters of the test procedure are defined as follows and can be visualized in supporting information S1:

- Slight overcharge via specification of charge amount (Ah-counter)
- Cycling range: 70 % - 130 % SOC
- C-rate: 3C
- Voltage limits: 1.5 V – 4.95 V
- Forced charge and discharge steps triggered by voltage limits: By reaching the voltage limits, cells are switched into the next charge or discharge step, respectively
- Cycling length: 1000 cycles consisting of 100 cycles blocks each followed by 1 h OCV-phase
- Temperature: Room temperature (defined as 22 °C)

2.4. Electrochemical check-up test for cells >1 Ah

To evaluate the damage done to the cell by the developed procedure an electrochemical test of cell capacity and direct current inner resistance was performed within the specified voltage windows of the cells before and after testing (see also supporting information S2 for measurement details). Therefore, charge was performed using a constant current (CC) constant voltage (CV) method (1C CC until upper voltage limit, CV until $I < C/20$) to reach 100 % SOC and discharge using CC of 1C until reaching lower voltage limit to determine the cell discharge capacity. Based on the measured discharge capacity of the cell and by use of an Ah counter method several state of charges (SOCs), namely 10 %, 30 %, 50 %, 70 % and 90 % were then adjusted. For these SOCs direct current (DC) internal resistances were determined by use of current pulses of 1C in discharge direction for 20 s. Applying Ohm's law, the DC internal resistances were determined using the potential drop (difference between the potential at the end of the pulse and the potential in rest state before the pulse) and the applied current for the respective pulses.

2.5. Cell inspection after testing

Formation of Li-plating was evaluated via optical *post*-mortem analysis. Cells were opened after testing under argon atmosphere. Microscopic images were taken directly after cell opening under dry room conditions (dew point temperature of −68 °C) to avoid decomposition reactions of metallic lithium.

3. Results and discussion

Inconsistencies and capacity fluctuations among cells in battery packs can easily lead to light overcharge during fast-charging [69–71], especially in case of serial connection. Therefore, two different test procedures were developed based on two light overcharge approaches. Cells were cycled using only constant current (CC) steps during charge and discharge. Several research activities have reported a pronounced increase in Li-plating at the anode surface particularly when charging the cell at high currents [48]. Thus, a C-rate of 3C was used for cycling.

3.1. Test development using lab-scale cells

Self-assembled, single-layer, lab-scale pouch cells were used for the development phase of the test procedures since these low-capacity cells render a moderate safety risk in case of thermal runaway. In addition, well-known cell components can be employed for the cell and materials of different quality can be implemented, avoiding deliberate cell manipulation through e.g., introduction of impurities. Further, these cells can be easily opened after testing to evaluate Li-plating. Cells based on graphite-anodes and NMC111-cathodes including polymeric and

ceramic-coated separators were investigated. However, only findings from cells including polymeric separators are discussed here in more detail since both cell types exhibit similar behavior (see supporting information S3–6).

3.1.1. Voltage-controlled procedure

First, cells were subjected to the voltage-controlled test procedure. As expected for a test with a specified voltage range (3.6 V – 4.5 V), the cell voltage response during cycling exhibits no mentionable irregularities over the 1000 cycles. As it has been reported before, a deviation from a monotonic decrease in voltage during the OCV-phase following a charging step can be a sign of Li-plating [52–57]. The voltage relaxation as a function of measuring time during an OCV-phase following a charge pulse in a series of each 100 cycles was recorded as a non-destructive, in-operando method to detect possible indications of Li-plating as shown in Fig. 1A. The OCV curves rapidly decrease shortly after the charge pulse and flatten after about 5 min, yielding a light decay over time. Especially after 500 cycles, the voltage curves tend to shift to higher values with increasing cycle number. It can be assumed that the internal cell resistance increases as a result of the demanding cycling conditions, leading to elevated voltage values. This effect is less pronounced in cells including a ceramic-coated separator (see supporting information S3 for direct comparison using the two different separator types). Interestingly, the voltage relaxation exhibits no sign of Li-plating as suggested by the monotonic decrease of the curve. Additionally, the Li-plating signature can also not be determined from the derivative of the voltage with respect to time. However, optical post-mortem analysis clearly shows formation of Li-plating over a large region of the anode surface (Fig. 1B). Elemental Li can even be found on the anode- as well as cathode- oriented side of the separator, suggesting Li dendrite growth through the separator and associated local short-circuits. Nevertheless, cells do not exhibit any indication of safety-critical behavior such as gas formation, mechanical deformation or overheating.

Cells including ceramic-coated separator exhibit an analogous behavior. However, lower amount of elemental Li can be observed on the anode, whereas larger areas of the separator show Li-deposits in a more homogeneous manner (see S4 for direct comparison of post-mortem images). It must be noted that the initial resistance of cells including both types of separators hardly differs and varies by 3 %–10 % depending on SOC, suggesting that the separator itself has an influence on Li-plating formation. Presumably, the shut-down mechanism of polymeric type separators closes the microstructure pores due to local heat generation, suppressing dendritic growth to the cathode side [72]. This might also explain such inhomogeneous lithiation and plating on the anode as indicated by the post-mortem inspection.

3.1.2. SOC-controlled procedure

In contrast to the voltage-controlled procedure, the voltage response of cells subjected to the SOC-controlled test exhibits a completely different behavior. In this case, tested cells only reached <200 cycles before the test had to be stopped due to significant voltage drop. Therefore, Li-plating could not be evaluated via voltage relaxation analysis, i.e., the voltage relaxation over time during the different OCV-steps could not be plotted. Instead, the actual voltage response during the procedure was plotted to characterize the cell behavior throughout the measurement as shown in Fig. 2A. Directly after test start, cell voltage steadily shifts to lower values with increasing measuring time or cycle number. At a critical point, the measurement was stopped in order to avoid a deep discharge of the cell as the voltage suddenly dropped towards 0 V (note that this low voltage most likely is induced by the high cell resistance such indicating a high over-voltage and in fact cell voltage relaxed during OCV). Subsequently, cell opening accompanied by microscopic images shows a massive amount of Li-plating on the surface of the anode as well as some elemental Li on both sides of the separator as indicated in Fig. 2B. Presumably, the drastic amount of elemental Li leads to the unusual voltage drop in the cell. It has been reported before that overcharge in the region between 120 %-140 % SOC might not only lead to significant Li-plating, but also trigger moderate side reactions such as dissolution of cathode material and electrolyte oxidation as well as increase of internal cell resistance and joule heating [45,73–76]. A more detailed investigation on the correlation between Li-plating and voltage drop will be discussed in the next section. Analog to cells subjected to the voltage-controlled procedure, the cells investigated here yield no mentionable safety-critical behavior, even though Li-plating covers most of the anode surface.

Similar to our findings for the voltage-controlled procedure, a more pronounced formation of Li-plating on the anode surface can be observed in cells including polymeric separators. Further, ceramic-coated separators exhibit larger traces of Li-plating than polymeric ones. Particularly for the SOC-controlled procedure, the overall amount of elemental Li on anode as well as separator surface is larger, despite shorter cycling of the cell. Naturally, the amount of Li-plating does not only correlate with cycle number but also with the specific overcharge protocol. Further, polymeric separators seem to hinder Li-dendrite deposit on, as well as growth through the separator, more effectively than ceramic-coated ones under the test conditions presented here. See

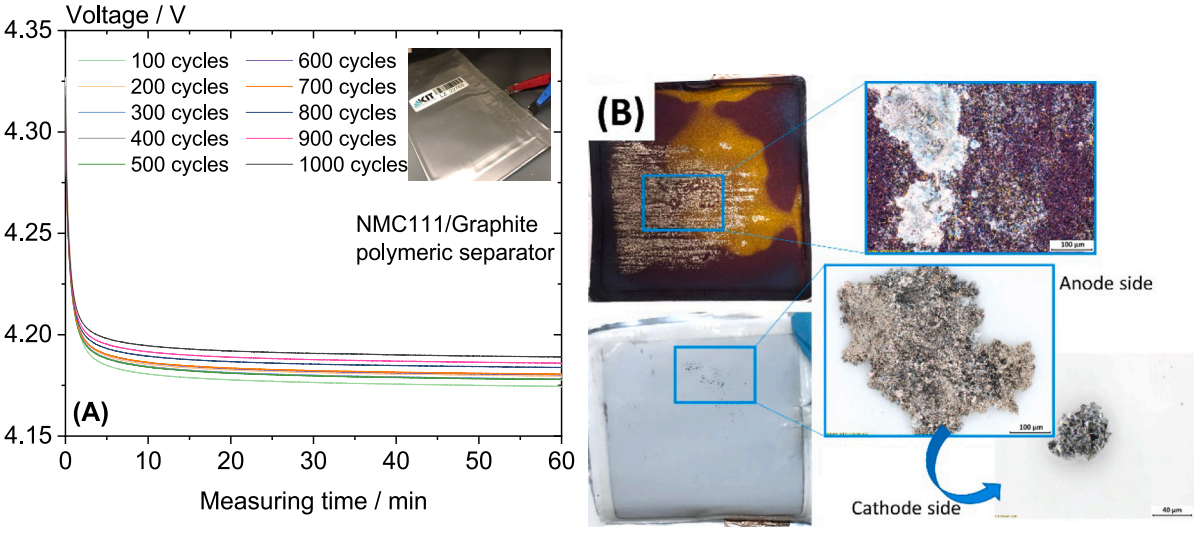

Fig. 1. (A) Voltage relaxation over measuring time during the OCV-phase every 100 cycles. Inset in (A) depicts a 44 mAh lab-scale pouch cell. (B) Anode and separator surface after cell testing.

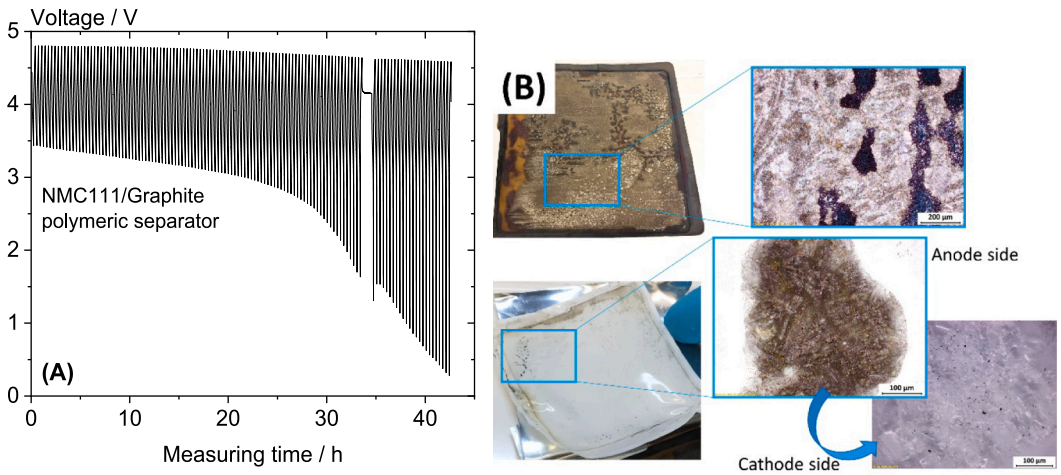

Fig. 2. (A) Voltage response over measuring time during cycling. (B) Anode and separator surface after cell testing.

supporting information for direct comparison of the cell's voltage response during SOC-controlled overcharge condition (S5), as well as the comparison of post-mortem findings (S6).

Both test procedures based on light overcharge, voltage- and SOC-controlled, lead to successful generation of an internal cell fault, namely Li-plating, in a reliable and reproducible manner. Elemental Li and associated dendrites were shown to have deposited on the anode surfaces with growth through the separator being visible on the cathode-oriented side in most tests, presumably causing localized short-circuits as well as localized heating. Even though both procedures successfully induce Li-plating, the electrical response of the cell during the voltage-controlled test does not clearly indicate if or when Li-plating has formed. Thus, Li-plating was solely detected by optical post-mortem analysis. On the other hand, the SOC-controlled procedure renders a more aggressive cycling approach, resulting in a stronger formation of elemental Li on anode and separator surfaces as confirmed by cell opening. In this case, the cell electrical response distinctly exhibits a critical point at which cell potential drops. This is assumed to be associated to specific side reactions in the cell triggered by Li-plating and its consequences such as enhanced internal resistance. M. Gonzalez et al. reported a voltage drop during the charging step for Li-metal cells [77]. However, the registered potential loss was attributed to internal shorting and accompanying cell self-discharge.

3.2. Test validation using technically relevant cells

Findings at lab-scale cell-level were validated using larger cells with technically relevant capacities. Self-assembled (KIT cells) 10 Ah and 12 Ah based on NMC111/Graphite and NMC622/Graphite, respectively, including polymeric as well as ceramic-coated separators as used in 3.1 were investigated. Additionally, commercial 3 Ah cylindrical 18,650 cells and 25 Ah pouch-cells were tested. All cells were subjected to both procedures, voltage- and SOC-controlled, although only the results of self-assembled cells based on NMC111/Graphite each with ceramic-coated and polymeric separator are closely discussed in this section. The results from testing the other cells are described within the supporting information (see S7). As described in Section 2.2, from this point on all cells were tested in the specially designed testing set-up, to guarantee safe conditions in case of an event.

In contrast to lab-scale cells, electrochemical properties (see Section 2.2 for details) as capacity, as well as internal resistance (RiDC) as a function of SOC, but also external cell aspects such as dimensions and weight were determined before and after testing to investigate the effect of the test procedure on internal and external cell parameters as well as to evaluate cell degradation.

3.2.1. Voltage-controlled procedure

Fig. 3 shows the voltage relaxation over time during the OCV-phase every 100 cycles (A) and the corresponding cell surface temperature (B) during voltage-controlled testing for a self-assembled KIT 10 Ah cell (NMC/Graphite) including ceramic-coated separator. Temperature sensors were evenly distributed on the cell surface (see Fig. 3B inset). Analog to lab-scale cells, the electrical cell response upon testing does not exhibit any sign of Li-plating as indicated by the monotonic voltage decay during the OCV phase after each 100 cycles block. Cell surface temperature yields no significant changes during cell operation. Hence, there is no evidence of Li-plating or safety-critical cell behavior. Nevertheless, cell characterization renders a slight increase in internal cell resistance as well as a capacity loss of about 12 % after the test. The charge amount measured from the Ah-counter during charge and discharge step continuously decreases with increasing cycle number (see S8), which can be associated to higher cell resistance values as well as Li-plating along other degradation mechanisms. Optical post-mortem analysis shows large amounts of elemental Li on the surface of anode and separator (see Fig. 3C). Li-dendrites could be found on the cathode-facing side of the separator as well. Accordingly, Li-plating cannot be reliably detected by the voltage profile during relaxation, confirming the limitation of this non-destructive approach despite its versatility and rather simple application [48,50].

3.2.2. SOC-controlled procedure

The investigation on lab-scale pouch-cells (44 mAh) showed a distinctive voltage drop for the SOC-controlled test procedure, risking deep discharge of the cell. Therefore, testing had to be stopped as cell voltage started to approach critically low values. For testing on large format cells, a lower limit voltage cutoff of 1.5 V was defined for termination of the test procedure. Fig. 4 displays the voltage (A) and cell surface temperature profile (B) over measuring time for a self-assembled KIT 10 Ah cell including polymeric separator. In the first cycle, cells were charged (CCCV) and discharged (CC) at 3C within their specified voltage window to determine cell capacity at the elevated C-rate. The exact state of charge was set via Ah-counter based on the measured initial 3C discharge capacity. Two reference cycles were subsequently run; first a full (100 % SOC) charge of the cell and then an overcharge (130 % SOC), each followed by an OCV-phase to record the voltage relaxation curve. Next, the cell was cycled within the SOC of 70–130 % SOC considering the 1.5 V lower boundary (see Section 2.3 for experimental details of the test protocol).

Analog to lab-scale pouch-cells, cell voltage decays monotonically over time and at a critical point it drops rapidly towards the lower voltage limit. In this case, a voltage increase over time can also be observed, especially directly prior to the voltage drop. At this critical

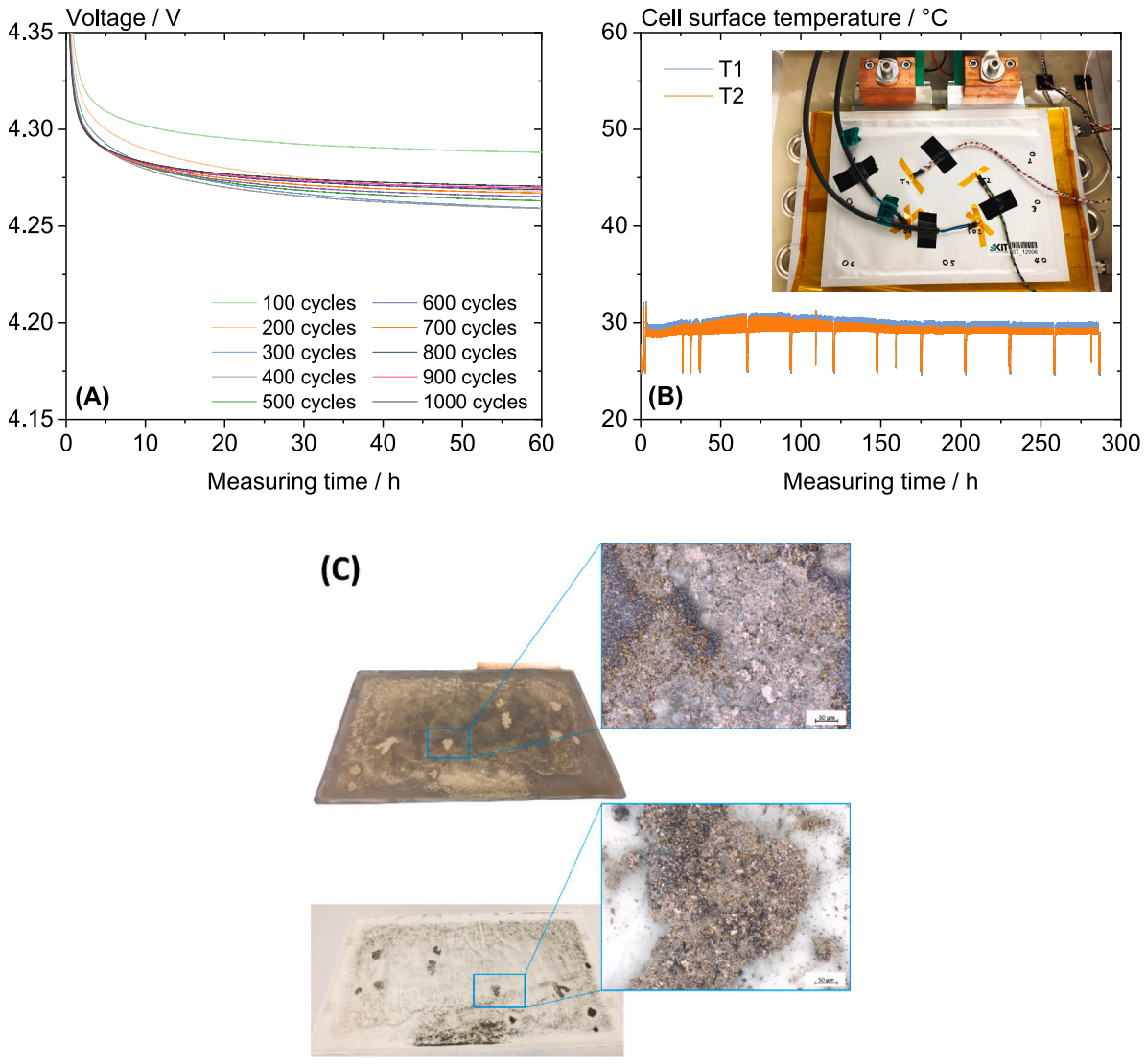

Fig. 3. (A) Voltage relaxation over measuring time during the OCV-phase every 100 cycles. (B) Cell surface temperature over measuring time. Inset in (B) illustrates the testing set-up of the cell including temperature sensors. (C) Optical post-mortem analysis of corresponding anode and ceramic-coated separator, indicating Li-plating.

point, cell temperature significantly increases, reaching about 50 °C. The voltage drop and accompanying temperature rise was observed for all investigated cells regardless of cell chemistry or cell format, rendering a general characteristic cell behavior upon SOC-controlled testing. This voltage and temperature response translates to an intensified cell degradation. Internal cell resistance dramatically increases by about 180 % on average for all SOC values, whereas cell capacity significantly decreases by about 36 %. It must be noted that the drastic cell degradation is achieved within the first 24 h of testing equivalent to <50 cycles. These findings are highlighted by the large amount of elemental Li on anode and separator surface as evidenced by optical post-mortem analysis (see Fig. 4C). Some Li-plating can be observed on the cathode side of the separator as well.

Contrary to lab-scale pouch-cells, there is no obvious difference between cells based on polymeric or ceramic-coated separators with respect to the amount of Li-plating located on anode and separator surface. Further, no evident contrast can be made out from the optical analysis between the voltage- and SOC-controlled procedure regarding the formation of Li-plating and dendrite growth, despite the clearly different voltage and temperature profile as well as degradation degree.

The investigation on large-format cells confirms our findings at lab-scale level, successfully validating the reliable and reproducible generation of Li-plating for both test procedures. This was corroborated on cells with different cell chemistries and formats. Table 1 summarizes the key cell parameters of all investigated cells applying the voltage- vs. SOC-controlled overcharge method. The highest increase in RiDC as well as capacity loss was determined for 25 Ah commercial pouch-cells based on NMC-blend and graphite, whereas 3 Ah cylindrical 18,650 cells including a NCA cathode exhibited the highest temperatures as expected for this cell type. These critical values were obtained when testing with the SOC-controlled procedure. Even though both procedures successfully induce Li-plating, the latter leads in most cases to overall higher temperatures as well as significantly higher cell degradation as indicated by the elevated internal cell resistance and capacity loss. Moreover, the SOC-controlled procedure renders a particular voltage behavior, i.e., potential drop, which seems to correlate with formation of Li-plating in the cell. Accordingly, elemental Li could be indirectly detected. Further, this method is not bound to specific operational voltages of cells with different chemistry since its approach is based on charge amount (Ah-counter), rendering a clear advantage over the voltage-controlled procedure regarding the applicability of the test to most cells. Although it is not the aim to force cell thermal runaway, this procedure enables

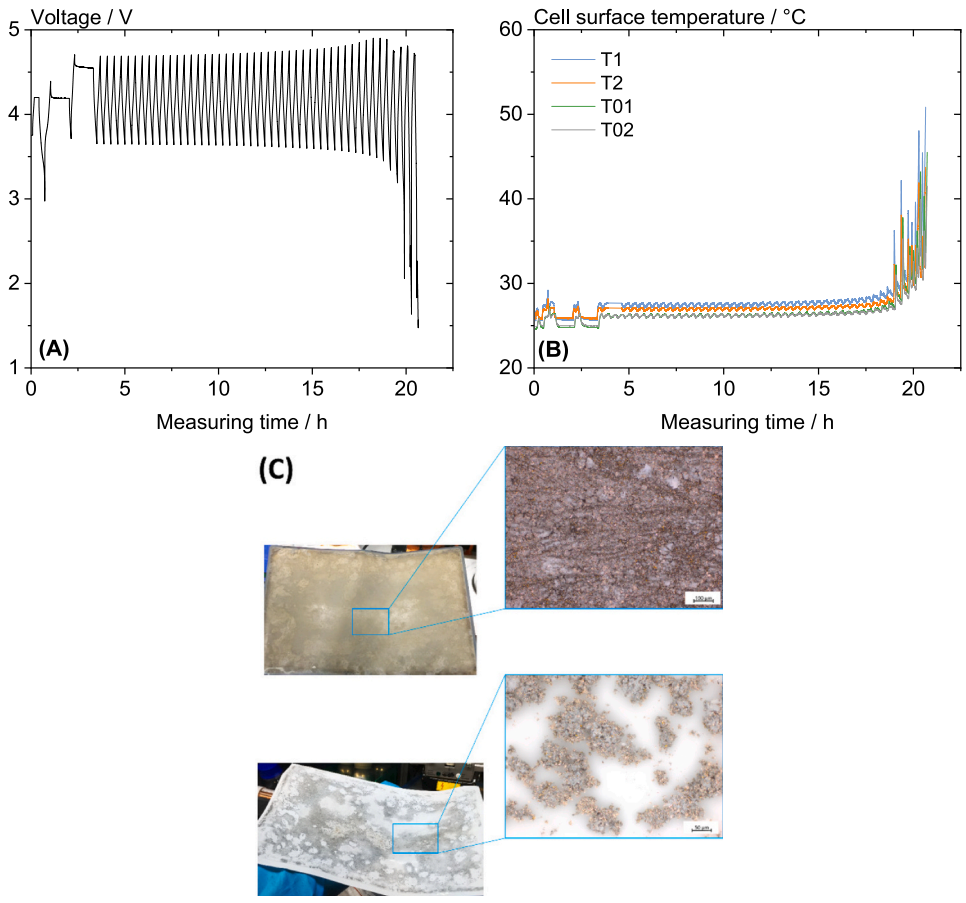

Fig. 4. (A) Voltage response over measuring time during cycling. (B) Cell surface temperature over measuring time. Inset in (B) illustrates the testing set-up of the cell including temperature sensors. (C) Optical post-mortem analysis of corresponding anode and ceramic-coated separator, indicating Li-plating.

Table 1
Summary of critical cell parameters of all investigated cells under the voltage- and SOC-controlled procedure.

Cell-type			Voltage-controlled			SOC-controlled		
Cathode active material, (separator)	Cell format, manufacturer	Nominal capacity	Max. temperature during test	RiDC increase[a]	Capacity loss	Max. temperature during test	RiDC increase[a]	Capacity loss
		[Ah]	[° C]	[%]	[%]	[° C]	[%]	[%]
NMC111 (Ceramic-coated)	Pouch, KIT	10	31	7 ± 3	12	37	77 ± 7	30
NMC111 (Polymeric)	Pouch, KIT	10	31	164 ± 22	51	51	179 ± 24	36
NMC622 (Ceramic-coated)	Pouch, KIT	12	32	10 ± 3	11	42	94 ± 23	39
NMC622 (Polymeric)	Pouch, KIT	12	32	19 ± 9	28	58	37 ± 11	25
NMC-blend (Ceramic-coated)	Pouch, commercial	25	30	4 ± 2	6	57	378 ± 40	48
NCA (unknown)	Cylindrical 18,650, commercial	3	56	20 ± 2	22	65	-[b]	-[b]

[a] Average over all corresponding SOC (10, 30, 50, 70, 90 %)-values.
[b] Test was stopped by the current interrupt device (CID) protection system, disabling the cell

evaluation of safety-critical cell behavior possibly allowing for identification of different cell quality and classification into different safety categories. Therefore, the SOC-driven test outstands as a more promising procedure to induce the targeted realistic consequences to an internal cell error.

3.3. Fine-tuning and definition of final test procedure

Further development activities to intensify the safety-critical behavior of cells upon testing with the SOC-controlled procedure were focused particularly on this method since it showed promising results during the conceptualization and validation phase. For this purpose, the voltage interruption criterion in the measurement plan was adjusted, keeping the cell from termination of the test when reaching 1.5 V lower

voltage limit. Instead, the cell was forced to recharge when this voltage was reached during the discharge step. Moreover, an upper voltage limit of 4.95 V was set in the charging direction as overcharge protection, whereby the cell was discharged again when this value was reached. Thus, cells were cycled between 70 % and 130 % SOC via Ah-counter, controlling the specific charge amount and imposing voltage limits, in which the cell was forced to cycle. The measuring protocol was designed with the aim that cells would always charge and discharge the same amount of charge per cycle (see also details in Section 2.3 and supporting information S1).

Additionally, further fine-tuning of the test procedure was probed to induce a more drastic cell response and facilitate cell classification. Measurement parameters and test conditions were varied to induce safety-critical cell behavior. The results of the following investigation were used to define the final version of the procedure.

First, self-assembled 12 Ah KIT-cells based on NMC622 and ceramic-coated separator were subjected to the adjusted test procedure at a measurement temperature of 10 °C instead of room temperature (see supporting information S9 for comparison of 10 vs. 22 °C). Cells tested at this temperature exhibit a decreased voltage drop and the evolution of cell temperature towards its maximum is slow but continuous, yet not critical. The temperature peak is nevertheless below the value obtained for cells tested at 22 °C. Thermograms show the steady heating of the cells surface with the continuous voltage drop. In addition, an inhomogeneous distribution of the temperature on the cell surface can be observed. Higher temperatures were detected in the immediate vicinity of the current collectors, whereas colder areas were observed at the edges and on the opposite side of the current collectors. Unfortunately, the assumption that lower experimental temperatures would lead to an intensified safety-critical cell behavior due to depleted ion diffusion and intercalation did not meet the expectations [19,78]. Instead, the cooling of the cell most likely counteracts the heat generation in the cell. Cells tested at an experimental temperature of 10 °C yield about 10 % less capacity loss than that of cells tested at 22 °C.

Furthermore, cells were braced between two aluminum plates and subjected to the test procedure to simulate the assembly situation in a cell pack or module. This additionally suppressed the swelling capability of the cell during the test. Self-assembled 12 Ah KIT-cells based on NMC622 cathode material and ceramic-coated as well as polymeric separators were investigated, both exhibiting similar behavior. The voltage response of braced cells does not significantly deviate from that of reference cells (see supporting information S10 for comparison). However, cell surface temperature of braced cells does not yield a steep rise during the voltage drop as known for reference cells. In addition, capacity loss after testing is significantly lower than that of reference cells. The bracing aluminum plates act as cooling plates, dissipating the generated heat. Accordingly, this assembly situation seems to have a counterproductive effect regarding safety-critical cell behavior, despite the suppression of cell swelling during testing.

Finally, cycling during the test procedure was performed at different C-rates (1C, 3C, 5C, 10C) to investigate its effect on cell behavior (see supporting information S11 for comparison of the results). Analog 12 Ah KIT-cells including NMC622 and both separator types were used. Both tested cells show similar behavior. The characteristic voltage drop shifts to higher measurement times with increasing C-rate. At a C-rate of 10C, the voltage drop is not observed. Cell surface temperature also yields a shift of the maximum value towards higher times corresponding to the shift of the voltage drop. The charge amount during testing, calculated from the Ah-counter, was analyzed to evaluate the voltage response as well as the temperature profile in more detail. The charge amount per cycle (charge/discharge step) before the voltage drop is significantly higher than after the voltage drop. Hence, the voltage drop divides the course of the charge amount into two regions. The region with high charge amount expands in accordance with the elapsed time before the voltage drop. Higher C-rates result in overall lower dis/charge amounts in the first region and this, in turn, leads to a delayed voltage drop accompanied by the onset of temperature rise. This effect is directly related to the measuring protocol, particularly to the determination of the initial cell capacity. The necessary charge amount to cycle the cell in the specific SOC range is determined from the cell discharge capacity (from a fully charged cell) at each investigated C-rate as described in 2.3 Therefore, cell capacity and associated charge amount per cycle decreases with increasing C-rate due to the prompt overvoltage during discharge at higher currents. The potentially enhanced safety-critical cell behavior induced by accelerated kinetics and associated intensified Li-plating at higher C-rates is suppressed by the reduced charge amount as a result of overvoltage during capacity determination. Cell degradation highlights these findings. Capacity loss decreases monotonically with increasing C-rate, whereas higher RiDC increment after testing was measured at lower C-rates. Contrary to expectations [63,79,80], high C-rates lead to lower degree of cell degradation under the specific parameters of the developed test procedure.

Low test temperature, bracing of the cell as well as high C-rates proved inefficient in respect to an enhanced safety-critical cell behavior. While a C-rate of 1C resulted in higher cell degradation, cells tested at 3C exhibited slightly higher cell surface temperatures. Furthermore, additional studies with LFP/Graphite and LCO/Graphite based cells showed a significantly more critical cell behavior when testing at 3C (results not shown here). According to these results the final version of the test procedure was defined as described in Section 2.3 and depicted in supporting information S1.

3.4. Cell behavior applying final test procedure

A last screening was carried out to evaluate the impact of the final test procedure on cells of different chemistry, processing, and quality. For convenience and better visualization, representative results of selected cells are discussed in more detail in the following. It must be noted that the reproducibility of the final test procedure was tested using three self-assembled KIT cells, rendering outstanding results, indicating remarkable reproducibility not only of the test but also of the self-manufactured cells (see supporting information S12). Fig. 5 displays the voltage response (A) and temperature profile (B) over measuring time as well as the SOC state per cycle (C) of a self-assembled 12 Ah KIT cell including NMC622/Graphite and polymeric separator. As expected, the voltage profile shows the characteristic voltage drop already in the first 24 h of cycling, which is associated to a rapid temperature rise of the cell surface. Cells, which were only cycled until this critical point, were opened and optically analyzed, evidencing large formations of Li-plating on anode and separator surface (see supporting information S13-S17). Cells, which were further cycled past the voltage drop according to the final test protocol, show a sequence of increasingly accelerated cycling behavior. The voltage response reaches the specified limits during every following cycle directly after the critical point. Each 100 cycles block runs for a shorter period than the latter, suggesting a steady increase of internal cell resistance or a continuously decreasing cell capacity with cycling. Both phenomena can be triggered by the strengthen generation of Li-plating with each charging step.

The SOC state, calculated from the Ah-counter per charge and discharge step, as a function of cycle number render further understanding on the cycling process and allows for a rough correlation with the voltage response and accompanying temperature profile. The KIT-cell runs within the specified SOC range (70 % - 130 %) for the first 50 cycles as shown in Fig. 5C. However, the covered SOC range promptly decreases within the next 7 cycles. This abrupt reduction in the covered SOC range correlates with the critical point denoted by voltage drop and temperature rise (respectively marked by a red dotted line). Particularly, the SOC state in the discharge direction increases significantly, indicating that the charge stored in the anode during the charge step cannot be extracted during the next discharging step, i.e., Li-ions cannot be deintercalated from the anode. Hence, a sudden increase in internal cell resistance is assumed, leading to over-potential during the discharge

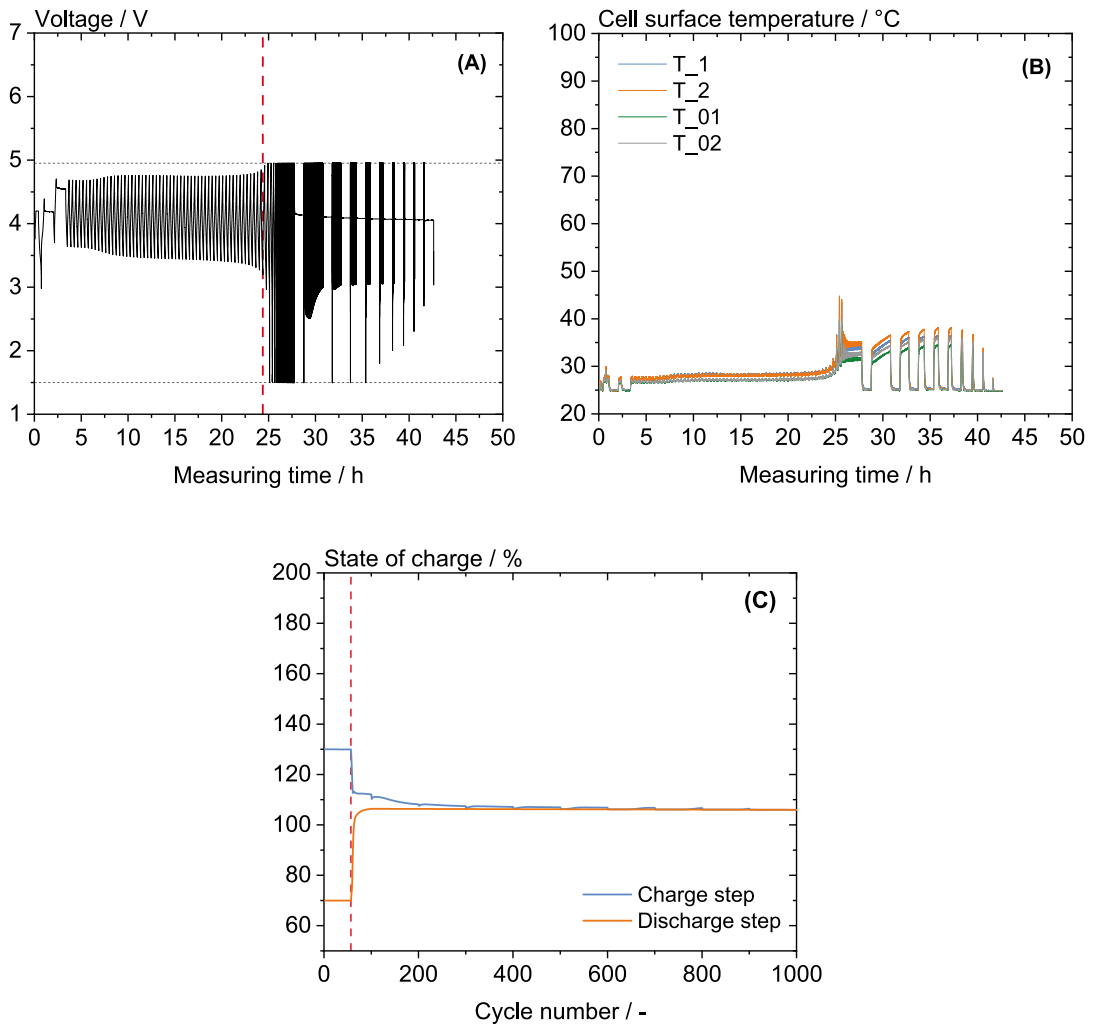

Fig. 5. (A) Voltage response over measuring time during cycling. (B) Cell surface temperature over measuring time. (C) SOC as a function of cycle number. A self-assembled 12 Ah pouch-cell including NMC622 and polymeric separator was used.

step, translating into the observed voltage drop. The SOC range converges from the critical point on, and a severely limited charge is added/removed from here on as reflected on the accelerated voltage response after the drop. It is clear that elemental Li gradually forms during the first cycles, not only reducing the available Li inventory, but also physically hindering ion deintercalation in the anode structure. This finding is in good agreement with the results reported by T. R. Tanim et al. [63]. Accordingly, it could be argued that the drop in cell potential provides a non-invasive, indirect indicator for Li-plating and resulting side reactions, leading to safety-critical cell behavior.

This final version of the test, rendering a more aggressive approach, leads to a tenfold higher internal cell resistance (RiDC) and a residual cell capacity of approx. 15 % after testing. This drastic cell degradation is attributed to massive generation of Li-plating on both, separator as well as anode surface and thus the side reactions triggered by the procedure. Remarkably, this KIT-cell exhibits no sign of safety-critical behavior.

A similar cell behavior, however, with considerably aggravated consequences with respect to cell safety, was found for commercial cells of different chemistry and processing. Fig. 6 shows the voltage response (A) and temperature profile (B) over measuring time as well as the SOC state per cycle (C) of a commercial 25 Ah pouch-cell based on an NMC-blend as cathode material. An image of the cell after testing is included as inset in Fig. 6B. The voltage response yields the characteristic profile with a voltage drop after about 85 cycles. At the same time, cell temperature significantly increases, reaching a maximum of approx. 100 °C. After only 30 cycles, the cell reaches the upper voltage limit, which correlates with a monotonic decrease in the upper SOC limit, i.e., the added charge during charging step. After 70 cycles, the decrease of the upper SOC limit accelerates, whereas cell potential rapidly decays towards 1.5 V, indicating a pronounced depletion of Li-ion de−/intercalation. The SOC values during charge and discharge step overlap at the critical point denoted by the voltage drop (respectively marked by a red dotted line). From this point on, no charge can be added or extracted from the anode as reflected in the pulsating voltage profile. Cell characterization after testing could not be carried out due to the large internal cell resistance. External cell damage was evident as the cell was clearly swollen, although no indication of venting was found.

Interestingly, LFP/Graphite based cells, which are often considered a “safe” chemistry, showed a more critical behavior as swelling and venting was triggered by the procedure (see supporting information S19). A venting scenario might be just as critical as an actual TR of the cell as local heat or spark within the battery would most probably ignite the highly volatile electrolyte solvents and thus, in turn, induce a cell fire after all, leading to propagation.

Ultimately, a commercial 50 Ah pouch-cell including NMC as cathode material was subjected to the test procedure. The corresponding voltage (A) and temperature profile (B) as well as the SOC range per cycle (C) are displayed in Fig. 7, exhibiting, as expected, a similar behavior as described before. However, this cell yields more drastic

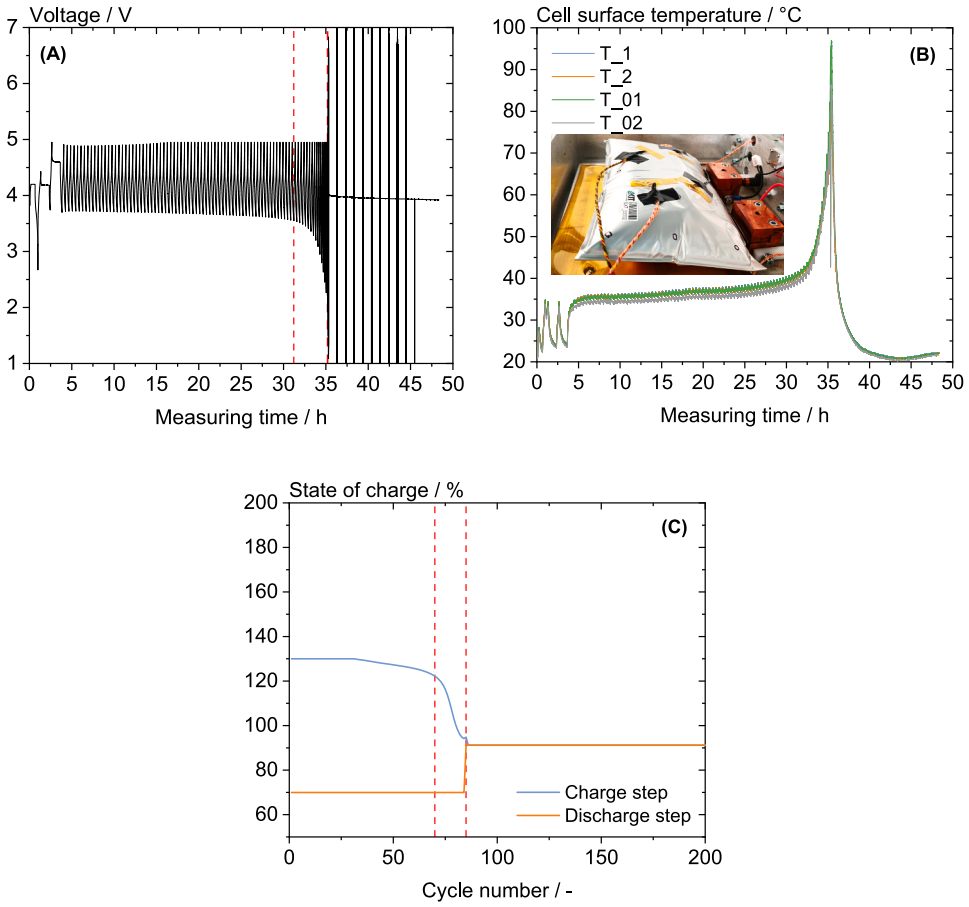

Fig. 6. (A) Voltage response over measuring time during cycling. (B) Cell surface temperature over measuring time with image of the cell after testing as inset. (C) SOC as a function of cycle number (reduced to 200 cycles for visualization). A commercial 25 Ah pouch-cell including NMC-blend as cathode material was used.

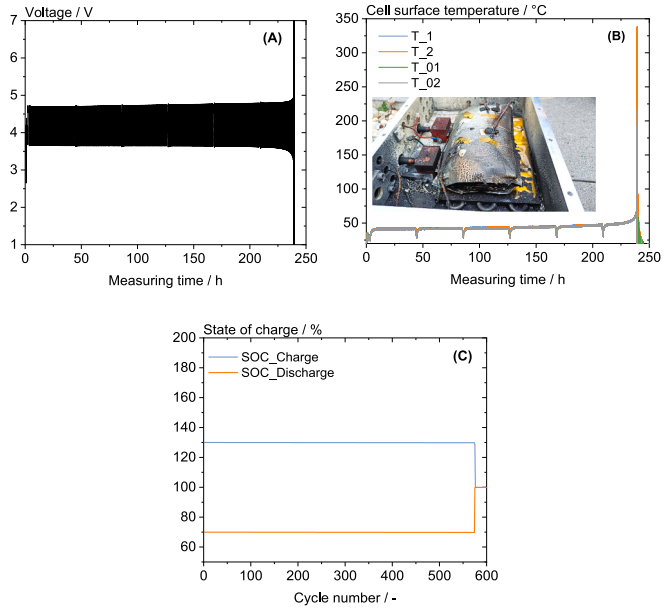

Fig. 7. (A) Voltage response over measuring time during cycling. (B) Cell surface temperature over measuring time with image of the cell after testing as inset. (C) SOC as a function of cycle number. A commercial 50 Ah pouch-cell including NMC as cathode material was used.

consequences upon testing. For over 500 cycles, this cell runs within the specified SOC-range without any mentionable changes in voltage or cell temperature. Nevertheless, the SOC-range spontaneously converges, suggesting a sudden limitation in Li-ion de−/intercalation, which in turn leads to over-potential and rapid temperature rise up to 350 °C. After opening the testing set-up, it was evident that the cell went into thermal runaway as shown in Fig. 7(B).

These findings clearly show that regardless of cathode chemistry, processing or quality all cells investigated here exhibit a common critical point, at which particularly the charge amount during the discharge step is suddenly limited, presumably, by the reduced Li-ion inventory and physical obstruction at the anode surface as a result of massive generation of Li-plating, leading to cell over-potential (referred to as voltage drop) and rapid temperature increase. Table 2 summarizes the critical parameters of all investigated cells under the final test procedure, highlighting the specific behavior of different cells, ranging from severe cell degradation without external damage over swelling and venting to thermal runaway. Detailed information for potential response, cell surface temperature charge amount, and optical cell inspection can be found in the supporting information for all cells (see S13-S20).

Regarding the implementation of the test procedure as a testing standard or normative document these findings allow for risk assessment and categorization of cells based on quality. Even though self-assembled KIT-cells yield high degradation ranging from 64 % to 94 % capacity loss upon testing, no critical safety behavior was observed. These cells, particularly cells including NMC622/Graphite, reach the critical point after relatively short measuring times i.e., after a few cycles. In this case, these cells do not represent a safety risk despite their quick and massive

Table 2
Summary of the critical test parameters of all investigated cells using the final version of the test procedure.

Cathode active material, (separator)	Cell format, manufacturer	Nominal capacity	Time to critical point	Cycle number to critical point	Max. temperature	Critical safety issues
		[Ah]	[h]	–	[° C]	–
NMC111 (Ceramic-coated)	Pouch, KIT	10	130	400	85	No
NMC111 (Polymeric)	Pouch, KIT	10	24	50	45	No
NMC622 (Ceramic-coated)	Pouch, KIT	12	4	3	65	No
NMC622 (Polymeric)	Pouch, KIT	12	4	3	60	No
NMC-blend (Ceramic-coated)	Pouch, commercial	25	35	85	100	Swelling
NMC (Ceramic-coated)	Pouch, commercial	50	240	575	350	Thermal runaway
LFP (unknown)	Pouch, commercial	3	5	10	85	Swelling + Venting
LCO (unknown)	Pouch, commercial	5	250	318	190	Thermal runaway

degradation. In contrast, most commercial cells investigated here could endure the abusive test for a longer period. Nevertheless, these cells exhibit physical degradation such as swelling and venting. Remarkably, the commercial 50 Ah pouch-cell reaches over 500 cycles before going into thermal runaway. The robustness of this cell must be highlighted despite the resulting critical safety behavior.

Clearly, cycling time before the critical point is reached and the resulting behavior should be defining parameters for cell classification and risk assessment within the framework of standardization.

4. Conclusions

This work introduces a novel test procedure to evaluate cell safety behavior under more realistic conditions based on the deliberate generation of Li-plating and its consequences as internal cell error. Therefore, two initial procedures on the basis of light overcharge, controlling the voltage window and the charge amount (SOC-region), were proposed and their ability to induce Li-plating was studied using self-assembled lab-scale pouch cells. Both procedures comprehensively proved to be successful in respect to the reliable and reproducible formation of elemental Li on the anode surface, with growth as dendrites through the separator and reaching the cathode side. These findings were validated on application-oriented self-assembled cells with technically relevant capacities as well as commercial cells, confirming the suitability of both approaches to induce an internal cell error and proof its response regarding cell safety.

Considering its higher impact on cell degradation, particularly on capacity loss and increase of internal cell resistance, the SOC-controlled procedure was fine-tuned, and a final version was proposed to intensify the impact of the test on the safety-critical behavior of the cell and evaluate the actual consequences of a common internal cell error, represented by Li-plating, and the thereby triggered side reactions, e.g., electrolyte degradation, inside the cell.

All cells subjected to the final version of the procedure render a distinctive response characterized by the sudden and rapid drop of cell voltage accompanied by a significant increase of cell temperature. This is most probably the cell reaction to critical internal cell resistance and a series of side reactions triggered by the loss of Li inventory on the cathode side as well as the electronically isolated plated Li, gradually formed during cycling, on the anode side, preventing delithiation of LiC_6 from local areas, as clearly indicated by the vast amount of deposited elemental Li on the anode and separator surface observed upon post-mortem analysis directly after the drop of cell potential. Despite the latter leading to massive cell degradation, safety behavior upon testing varies depending on cell composition and quality as heat capacity of cell components are responsible for heat dissipation, depicting the consequences to an internal cell error closer to reality, in contrast to currently used testing protocols.

Accordingly, the test procedure presented here offers the possibility for risk assessment as well as cell categorization and shows great potential to be used as trigger method for a propagation test since it can be directly applied on an electrically connected cell within a battery system. In addition, the test procedure does not need further equipment beyond a potentiostat, highlighting its straightforward implementation in testing laboratories.

Finally, this work provides new insights into the real outcome of Li-plating and dendrite growth in respect to cell safety, clearly demonstrating that this parasitic phenomenon does not necessarily lead to a short-circuit as it has been assumed before and even in this case the latter does not automatically result in a critical safety issue such as thermal runaway. Moreover, the consequences of the lithium plating as stated above result in critical behavior of the cell.

Future work will focus on the extensive testing of several more cells to expand our data base, allowing for possible identification of trends among cell components/quality and resulting safety behavior. Moreover, testing at pack and module level will be carried out to address propagation. Conclusively, the developed procedure will be introduced as a normative document to facilitate use and safety regulation of batteries.

CRediT authorship contribution statement

Ronald Gordon: Conceptualization, Methodology, Validation, Formal analysis, Investigation, Writing – original draft, Visualization. **Anna Smith:** Conceptualization, Methodology, Writing – review & editing, Project administration.

Declaration of competing interest

The authors declare that they have no known competing financial interests or personal relationships that could have appeared to influence the work reported in this paper.

Data availability

Data will be made available on request.

Acknowledgements

This work was funded by the Federal Ministry for Economic Affairs

and Climate Action (BMWK) under the ProLIB project (03EI3003A). The authors express their gratitude for the financial support. Moreover, special thanks are denoted to Olivia Wiegand for cell fabrication and to Steffen Jokisch for his remarkable experimental assistance and technical support. The cell assembling was done at KIT Battery Technology Center (KIT-BATEC) and contributes to the research performed at the Center for Electrochemical Energy Storage Ulm & Karlsruhe (CELEST).

Appendix A. Supplementary data

Supplementary data to this article can be found online at https://doi.org/10.1016/j.est.2023.108200.

References

[1] B. Dunn, H. Kamath, J.-M. Tarascon, Electrical energy storage for the grid: a battery of choices, Science (80) 334 (6058) (2011) 928–935. Nov. https://doi.org/10.1126/science.1212741. Nov.
[2] X. Luo, J. Wang, M. Dooner, J. Clarke, Overview of current development in electrical energy storage technologies and the application potential in power system operation, Appl. Energy 137 (2015) 511–536, https://doi.org/10.1016/j.apenergy.2014.09.081.
[3] D. Deng, Li-ion batteries: basics, progress, and challenges, Energy Sci. Eng. 3 (5) (2015) 385–418, https://doi.org/10.1002/ese3.95.
[4] G.E. Blomgren, The development and future of Lithium ion batteries, J. Electrochem. Soc. 164 (1) (2017) A5019–A5025, https://doi.org/10.1149/2.0251701jes.
[5] C.T. Love, C. Buesser, M.D. Johannes, K.E. Swider-Lyons, Innovating safe lithium-ion batteries through basic to applied research, J. Electrochem. Energy Convers. Storage 15 (1) (Feb. 2018), https://doi.org/10.1115/1.4038075.
[6] D.P. Finegan, et al., Identifying the cause of rupture of Li-ion batteries during thermal runaway, Adv. Sci. 5 (1) (Jan. 2018) 1700369, https://doi.org/10.1002/advs.201700369.
[7] B. Liu, J. Zhang, C. Zhang, J. Xu, Mechanical integrity of 18650 lithium-ion battery module: packing density and packing mode, Eng. Fail. Anal. 91 (2018) 315–326. Sep. https://doi.org/10.1016/j.engfailanal.2018.04.041. Sep.
[8] X. Feng, M. Ouyang, X. Liu, L. Lu, Y. Xia, X. He, Thermal runaway mechanism of lithium ion battery for electric vehicles: a review, Energy Storage Mater. 10 (2018) 246–267. Jan. https://doi.org/10.1016/j.ensm.2017.05.013. Jan.
[9] Z. Chen, R. Xiong, J. Lu, X. Li, Temperature rise prediction of lithium-ion battery suffering external short circuit for all-climate electric vehicles application, Appl. Energy 213 (2018) 375–383. Mar. https://doi.org/10.1016/j.apenergy.2018.01.068.
[10] Y. Chen, et al., A review of lithium-ion battery safety concerns: the issues, strategies, and testing standards, J. Energy Chem. 59 (2021) 83–99, https://doi.org/10.1016/j.jechem.2020.10.017.
[11] V. Ruiz, A. Pfrang, A. Kriston, N. Omar, P. Van den Bossche, L. Boon-Brett, A review of international abuse testing standards and regulations for lithium ion batteries in electric and hybrid electric vehicles, Renew. Sust. Energ. Rev. 81 (May 2017) (2018) 1427–1452, https://doi.org/10.1016/j.rser.2017.05.195.
[12] S. Koch, A. Fill, K.P. Birke, Comprehensive gas analysis on large scale automotive lithium-ion cells in thermal runaway, J. Power Sources 398 (Sep. 2018) 106–112, https://doi.org/10.1016/j.jpowsour.2018.07.051.
[13] F. Larsson, P. Andersson, P. Blomqvist, B.-E. Mellander, Toxic fluoride gas emissions from lithium-ion battery fires, Sci. Rep. 7 (1) (Dec. 2017) 10018, https://doi.org/10.1038/s41598-017-09784-z.
[14] F. Larsson, S. Bertilsson, M. Furlani, I. Albinsson, B.E. Mellander, Gas explosions and thermal runaways during external heating abuse of commercial lithium-ion graphite-LiCoO2 cells at different levels of ageing, J. Power Sources 373 (July 2017) (2018) 220–231, https://doi.org/10.1016/j.jpowsour.2017.10.085.
[15] P.V. Chombo, Y. Laoonual, A review of safety strategies of a Li-ion battery, J. Power Sources 478 (July) (2020), https://doi.org/10.1016/j.jpowsour.2020.228649.
[16] S.S. Choi, H.S. Lim, Factors that affect cycle-life and possible degradation mechanisms of a Li-ion cell based on LiCoO2, J. Power Sources 111 (1) (2002) 130–136, https://doi.org/10.1016/S0378-7753(02)00305-1.
[17] M. Broussely, et al., Main aging mechanisms in Li ion batteries, J. Power Sources 146 (1–2) (2005) 90–96, https://doi.org/10.1016/j.jpowsour.2005.03.172.
[18] A.M. Andersson, M. Herstedt, A.G. Bishop, K. Edström, The influence of lithium salt on the interfacial reactions controlling the thermal stability of graphite anodes, Electrochim. Acta 47 (12) (2002) 1885–1898, https://doi.org/10.1016/S0013-4686(02)00044-0.
[19] K. Jalkanen, J. Karppinen, L. Skogström, T. Laurila, M. Nisula, K. Vuorilehto, Cycle aging of commercial NMC/graphite pouch cells at different temperatures, Appl. Energy 154 (2015) 160–172, https://doi.org/10.1016/j.apenergy.2015.04.110.
[20] C.R. Birkl, M.R. Roberts, E. McTurk, P.G. Bruce, D.A. Howey, Degradation diagnostics for lithium ion cells, J. Power Sources 341 (2017) 373–386, https://doi.org/10.1016/j.jpowsour.2016.12.011.
[21] J. Vetter, et al., Ageing mechanisms in lithium-ion batteries, J. Power Sources 147 (1–2) (2005) 269–281, https://doi.org/10.1016/j.jpowsour.2005.01.006.
[22] M.M. Kabir, D.E. Demirocak, Degradation mechanisms in Li-ion batteries: a state-of-the-art review, Int. J. Energy Res. 41 (14) (Nov. 2017) 1963–1986, https://doi.org/10.1002/er.3762.
[23] S.C. Nagpure, B. Bhushan, S.S. Babu, Multi-scale characterization studies of aged Li-ion large format cells for improved performance: an overview, J. Electrochem. Soc. 160 (11) (2013) A2111–A2154, https://doi.org/10.1149/2.001311jes.
[24] A. Mukhopadhyay, B.W. Sheldon, Deformation and stress in electrode materials for Li-ion batteries, Prog. Mater. Sci. 63 (January) (2014) 58–116, https://doi.org/10.1016/j.pmatsci.2014.02.001.
[25] S. Ramdon, B. Bhushan, Nanomechanical characterization and mechanical integrity of unaged and aged Li-ion battery cathodes, J. Power Sources 246 (2014) 219–224, https://doi.org/10.1016/j.jpowsour.2013.07.078.
[26] R. Stockhausen, et al., Investigating the dominant decomposition mechanisms in lithium-ion battery cells responsible for capacity loss in different stages of electrochemical aging, J. Power Sources 543 (Sep. 2022), https://doi.org/10.1016/j.jpowsour.2022.231842.
[27] M. Chen, et al., A large-scale experimental study on the thermal failure propagation behaviors of primary lithium batteries, J. Energy Storage 31 (July) (2020), 101657, https://doi.org/10.1016/j.est.2020.101657.
[28] Z. Wang, T. He, H. Bian, F. Jiang, Y. Yang, Characteristics of and factors influencing thermal runaway propagation in lithium-ion battery packs, J. Energy Storage 41 (Sep. 2021), 102956, https://doi.org/10.1016/j.est.2021.102956.
[29] Z. Huang, et al., Experimental investigation on thermal runaway propagation of large format lithium ion battery modules with two cathodes, Int. J. Heat Mass Transf. 172 (Jun. 2021), 121077, https://doi.org/10.1016/j.ijheatmasstransfer.2021.121077.
[30] C. Xu, et al., Experimental study on thermal runaway propagation of lithium-ion battery modules with different parallel-series hybrid connections, J. Clean. Prod. 284 (Feb. 2021), 124749, https://doi.org/10.1016/j.jclepro.2020.124749.
[31] J. Lamb, C.J. Orendorff, L.A.M. Steele, S.W. Spangler, Failure propagation in multi-cell lithium ion batteries, J. Power Sources 283 (2015) 517–523, https://doi.org/10.1016/j.jpowsour.2014.10.081.
[32] D.P. Finegan, et al., Characterising thermal runaway within lithium-ion cells by inducing and monitoring internal short circuits, Energy Environ. Sci. 10 (6) (2017) 1377–1388, https://doi.org/10.1039/c7ee00385d.
[33] B. Liu, et al., Safety issues and mechanisms of lithium-ion battery cell upon mechanical abusive loading: a review, Energy Storage Mater. 24 (June) (2020) 85–112, https://doi.org/10.1016/j.ensm.2019.06.036.
[34] X. Feng, et al., Characterization of penetration induced thermal runaway propagation process within a large format lithium ion battery module, J. Power Sources 275 (2015) 261–273, https://doi.org/10.1016/j.jpowsour.2014.11.017.
[35] T. Kisters, E. Sahraei, T. Wierzbicki, Dynamic impact tests on lithium-ion cells, Int. J. Impact Eng. 108 (2017) 205–216. Oct. https://doi.org/10.1016/j.ijimpeng.2017.04.025.
[36] P. Ping, D. Kong, J. Zhang, R. Wen, J. Wen, Characterization of behaviour and hazards of fire and deflagration for high-energy Li-ion cells by over-heating, J. Power Sources 398 (Sep. 2018) 55–66, https://doi.org/10.1016/j.jpowsour.2018.07.044.
[37] H. Wang, W. Shi, F. Hu, Y. Wang, X. Hu, H. Li, Over-heating triggered thermal runaway behavior for lithium-ion battery with high nickel content in positive electrode, Energy 224 (Jun. 2021), 120072, https://doi.org/10.1016/j.energy.2021.120072.
[38] D. Ren, X. Feng, L. Lu, X. He, M. Ouyang, Overcharge behaviors and failure mechanism of lithium-ion batteries under different test conditions, Appl. Energy 250 (Sep. 2019) 323–332, https://doi.org/10.1016/j.apenergy.2019.05.015.
[39] J. Liu, Q. Duan, M. Ma, C. Zhao, J. Sun, Q. Wang, Aging mechanisms and thermal stability of aged commercial 18650 lithium ion battery induced by slight overcharging cycling, J. Power Sources 445 (Jan. 2020) 227263, https://doi.org/10.1016/j.jpowsour.2019.227263.
[40] J. Hong, et al., Investigation on overcharge-caused thermal runaway of lithium-ion batteries in real-world electric vehicles, Appl. Energy 321 (Sep. 2022) 119229, https://doi.org/10.1016/j.apenergy.2022.119229.
[41] N. Legrand, B. Knosp, P. Desprez, F. Lapicque, S. Raël, Physical characterization of the charging process of a Li-ion battery and prediction of Li plating by electrochemical modelling, J. Power Sources 245 (Jan. 2014) 208–216, https://doi.org/10.1016/j.jpowsour.2013.06.130.
[42] T. Gao, et al., Interplay of lithium intercalation and plating on a single graphite particle, Joule 5 (2) (Feb. 2021) 393–414, https://doi.org/10.1016/j.joule.2020.12.020.
[43] X.-L. Gao, X.-H. Liu, W.-L. Xie, L.-S. Zhang, S.-C. Yang, Multiscale observation of Li plating for lithium-ion batteries, Rare Metals 40 (11) (Nov. 2021) 3038–3048, https://doi.org/10.1007/s12598-021-01730-3.
[44] W. Mei, L. Jiang, C. Liang, J. Sun, Q. Wang, Understanding of Li-plating on graphite electrode: detection, quantification and mechanism revelation, Energy Storage Mater. 41 (Oct. 2021) 209–221, https://doi.org/10.1016/j.ensm.2021.06.013.
[45] W. Cai, et al., The boundary of Lithium plating in graphite electrode for safe Lithium-ion batteries, Angew. Chem. Int. Ed. 60 (23) (Jun. 2021) 13007–13012, https://doi.org/10.1002/anie.202102593.
[46] T. Waldmann, B.-I. Hogg, M. Wohlfahrt-Mehrens, Li plating as unwanted side reaction in commercial Li-ion cells – a review, J. Power Sources 384 (Apr. 2018) 107–124, https://doi.org/10.1016/j.jpowsour.2018.02.063.
[47] S.-B. Son, D. Robertson, Z. Yang, Y. Tsai, S. Lopykinski, I. Bloom, Fast charge-driven Li plating on anode and structural degradation of cathode, J. Electrochem. Soc. 167 (14) (Oct. 2020), 140506, https://doi.org/10.1149/1945-7111/abc031.

[48] A. Tomaszewska, et al., Lithium-ion battery fast charging: a review, eTransportation 1 (2019), 100011, https://doi.org/10.1016/j.etran.2019.100011.
[49] J. Betz, G. Bieker, P. Meister, T. Placke, M. Winter, R. Schmuch, Theoretical versus practical energy: a Plea for more transparency in the energy calculation of different rechargeable battery systems, Adv. Energy Mater. 9 (6) (2019), https://doi.org/10.1002/aenm.201803170.
[50] P.P. Paul, et al., A review of existing and emerging methods for lithium detection and characterization in Li-ion and Li-metal batteries, Adv. Energy Mater. (2021), https://doi.org/10.1002/aenm.202100372.
[51] F. Sagane, R. Shimokawa, H. Sano, H. Sakaebe, Y. Iriyama, In-situ scanning electron microscopy observations of Li plating and stripping reactions at the lithium phosphorus oxynitride glass electrolyte/cu interface, J. Power Sources 225 (Mar. 2013) 245–250, https://doi.org/10.1016/j.jpowsour.2012.10.026.
[52] Z.M. Konz, E.J. McShane, B.D. McCloskey, Detecting the onset of lithium plating and monitoring fast charging performance with voltage relaxation, ACS Energy Lett. 5 (6) (Jun. 2020) 1750–1757, https://doi.org/10.1021/acsenergylett.0c00831.
[53] S. Schindler, M. Bauer, M. Petzl, M.A. Danzer, Voltage relaxation and impedance spectroscopy as in-operando methods for the detection of lithium plating on graphitic anodes in commercial lithium-ion cells, J. Power Sources 304 (2016) 170–180, https://doi.org/10.1016/j.jpowsour.2015.11.044.
[54] C. Uhlmann, J. Illig, M. Ender, R. Schuster, E. Ivers-Tiffée, In situ detection of lithium metal plating on graphite in experimental cells, J. Power Sources 279 (Apr. 2015) 428–438, https://doi.org/10.1016/j.jpowsour.2015.01.046.
[55] D. Ren, et al., Investigation of Lithium plating-stripping process in Li-ion batteries at low temperature using an electrochemical model, J. Electrochem. Soc. 165 (10) (Jul. 2018) A2167–A2178, https://doi.org/10.1149/2.0661810jes.
[56] X.-G. Yang, S. Ge, T. Liu, Y. Leng, C.-Y. Wang, A look into the voltage plateau signal for detection and quantification of lithium plating in lithium-ion cells, J. Power Sources 395 (Aug. 2018) 251–261, https://doi.org/10.1016/j.jpowsour.2018.05.073.
[57] C. Fear, T. Adhikary, R. Carter, A.N. Mistry, C.T. Love, P.P. Mukherjee, In operando detection of the onset and mapping of Lithium plating regimes during fast charging of lithium-ion batteries, ACS Appl. Mater. Interfaces 12 (27) (Jul. 2020) 30438–30448, https://doi.org/10.1021/acsami.0c07803.
[58] O. Crowther, A.C. West, Effect of electrolyte composition on Lithium dendrite growth, J. Electrochem. Soc. 155 (11) (2008) A806, https://doi.org/10.1149/1.2969424.
[59] A. Aryanfar, D.J. Brooks, A.J. Colussi, M.R. Hoffmann, Quantifying the dependence of dead lithium losses on the cycling period in lithium metal batteries, Phys. Chem. Chem. Phys. 16 (45) (2014) 24965–24970, https://doi.org/10.1039/C4CP03590A.
[60] Z. Guo, J. Zhu, J. Feng, S. Du, Direct in situ observation and explanation of lithium dendrite of commercial graphite electrodes, RSC Adv. 5 (85) (2015) 69514–69521, https://doi.org/10.1039/C5RA13289D.
[61] J. Steiger, G. Richter, M. Wenk, D. Kramer, R. Mönig, Comparison of the growth of lithium filaments and dendrites under different conditions, Electrochem. Commun. 50 (Jan. 2015) 11–14, https://doi.org/10.1016/j.elecom.2014.11.002.
[62] G. Bieker, M. Winter, P. Bieker, Electrochemical in situ investigations of SEI and dendrite formation on the lithium metal anode, Phys. Chem. Chem. Phys. 17 (14) (2015) 8670–8679, https://doi.org/10.1039/C4CP05865H.
[63] T.R. Tanim, et al., Heterogeneous behavior of Lithium plating during extreme fast charging, Cell Rep. Phys. Sci. 1 (7) (2020), https://doi.org/10.1016/j.xcrp.2020.100114.
[64] J.C. Burns, D.A. Stevens, J.R. Dahn, In-situ detection of Lithium plating using high precision coulometry, J. Electrochem. Soc. 162 (6) (Mar. 2015) A959–A964, https://doi.org/10.1149/2.0621506jes.
[65] B. Bitzer, A. Gruhle, A new method for detecting lithium plating by measuring the cell thickness, J. Power Sources 262 (2014) 297–302, https://doi.org/10.1016/j.jpowsour.2014.03.142.
[66] M. Bauer, M. Wachtler, H. Stöwe, J.V. Persson, M.A. Danzer, Understanding the dilation and dilation relaxation behavior of graphite-based lithium-ion cells, J. Power Sources 317 (Jun. 2016) 93–102, https://doi.org/10.1016/j.jpowsour.2016.03.078.
[67] A. Adam, J. Wandt, E. Knobbe, G. Bauer, A. Kwade, Fast-charging of automotive lithium-ion cells: in-situ lithium-plating detection and comparison of different cell designs, J. Electrochem. Soc. 167 (13) (2020), 130503. Sep. https://doi.org/10.1149/1945-7111/abb564. Sep.
[68] O. Pecher, J. Carretero-González, K.J. Griffith, C.P. Grey, Materials' methods: NMR in battery research, Chem. Mater. 29 (1) (Jan. 2017) 213–242, https://doi.org/10.1021/acs.chemmater.6b03183.
[69] T.R. Tanim, M.G. Shirk, R.L. Bewley, E.J. Dufek, B.Y. Liaw, Fast charge implications: pack and cell analysis and comparison, J. Power Sources 381 (Mar. 2018) 56–65, https://doi.org/10.1016/j.jpowsour.2018.01.091.
[70] C. Zhang, Y. Jiang, J. Jiang, G. Cheng, W. Diao, W. Zhang, Study on battery pack consistency evolutions and equilibrium diagnosis for serial- connected lithium-ion batteries, Appl. Energy 207 (Dec. 2017) 510–519, https://doi.org/10.1016/j.apenergy.2017.05.176.
[71] Z. Li, L. Lu, M. Ouyang, Y. Xiao, Modeling the capacity degradation of LiFePO4/graphite batteries based on stress coupling analysis, J. Power Sources 196 (22) (Nov. 2011) 9757–9766, https://doi.org/10.1016/j.jpowsour.2011.07.080.
[72] I.A. Shkrob, M. Luo, M.T.F. Rodrigues, S.E. Trask, D.P. Abraham, Fast charging of Li-ion cells: effect of separator membranes and mapping of 'safe lines' to avoid Li plating, J. Power Sources 549 (Nov. 2022), https://doi.org/10.1016/j.jpowsour.2022.232086.
[73] D. Ren, et al., An electrochemical-thermal coupled overcharge-to-thermal-runaway model for lithium ion battery, J. Power Sources 364 (Oct. 2017) 328–340, https://doi.org/10.1016/j.jpowsour.2017.08.035.
[74] H. Zheng, Q. Sun, G. Liu, X. Song, V.S. Battaglia, Correlation between dissolution behavior and electrochemical cycling performance for LiNi1/3Co1/3Mn1/3O2-based cells, J. Power Sources 207 (Jun. 2012) 134–140, https://doi.org/10.1016/j.jpowsour.2012.01.122.
[75] N. Sharma, V.K. Peterson, Overcharging a lithium-ion battery: effect on the LixC6 negative electrode determined by in situ neutron diffraction, J. Power Sources 244 (Dec. 2013) 695–701, https://doi.org/10.1016/j.jpowsour.2012.12.019.
[76] S. Santhanagopalan, P. Ramadass, J. (Zhengming) Zhang, Analysis of internal short-circuit in a lithium ion cell, J. Power Sources 194 (1) (Oct. 2009) 550–557, https://doi.org/10.1016/j.jpowsour.2009.05.002.
[77] M.S. Gonzalez, et al., Draining over blocking: nano-composite janus separators for mitigating internal shorting of lithium batteries, Adv. Mater. 32 (12) (Mar. 2020), https://doi.org/10.1002/adma.201906836.
[78] T. Waldmann, M. Wilka, M. Kasper, M. Fleischhammer, M. Wohlfahrt-Mehrens, Temperature dependent ageing mechanisms in lithium-ion batteries - a post-mortem study, J. Power Sources 262 (2014) 129–135, https://doi.org/10.1016/j.jpowsour.2014.03.112.
[79] A. Meintz, et al., Enabling fast charging – vehicle considerations, J. Power Sources 367 (Nov. 2017) 216–227, https://doi.org/10.1016/j.jpowsour.2017.07.093.
[80] A. Schmidt, A. Smith, H. Ehrenberg, Power capability and cyclic aging of commercial, high power lithium ion battery cells with respect to different cell designs, J. Power Sources 425 (Jun. 2019) 27–38, https://doi.org/10.1016/j.jpowsour.2019.03.075.